RECENT FLOW ANALYSIS STUDIES IN VASCULAR MODELS USING DOPPLER ULTRASOUND

Tamie L. Poepping[1,2], Meghan L. Thorne[2,4], Emily Y. Wong[2,4], Richard N. Rankin[3], and David W. Holdsworth[3,4]
Depts of Physics & Astronomy1, Medical Biophysics2, and Diagnostic Radiology & Nuclear Medicine3, at the University of Western Ontario, London, ON N6A 3K7; and The Robarts Research Institute4, 100 Perth Drive, London, ON, N6A 5K8

ABSTRACT

Vascular disease is a major source of morbidity and mortality in Western society, with stroke and heart attacks accounting for about one third of deaths in North America. The carotid artery, and in particular the carotid bifurcation, is recognized as a common source of stroke-causing emboli that travel up into the brain, thereby blocking local blood flow. This has led to an emphasis on diagnostic techniques for assessing stroke risk due to carotid artery disease. Doppler ultrasound (DUS) techniques, in particular, uniquely enable visualization of flow patterns and characterization of various flow parameters. To improve our understanding of how blood-flow velocity patterns are modified as a result of disease in the carotid artery, basic research is typically carried out in physiologically realistic vascular models. In this paper, we review the progress that has been made in the development of ultrasound-compatible vascular models, as well as demonstrate the capabilities of DUS to quantify velocity patterns, turbulence, and recirculation. Ultrasound-compatible flow systems have been developed to mimic the geometry and hemodynamics of the carotid artery, under normal conditions and at various stages of narrowing due to atherosclerosis. These in vitro systems provide a controlled environment for developing new diagnostic techniques and for investigating and characterizing blood flow using DUS. Example data are shown from vessels with both eccentric and concentric stenoses, and in stenosed vessels that have been altered by the introduction of medical devices (stents) or additional roughness (ulceration). These results demonstrate the capacity for conventional clinical Doppler ultrasound devices to provide precise measurements of blood velocity from small sample volumes within a vessel, in order to build up detailed flow maps near and downstream of vascular disease or interventional device.

SOMMAIRE

Les maladies vasculaires sont une source importante de morbidité et de mortalité dans la société occidentale. Les accidents cérébrovasculaires et les crises cardiaques sont responsables pour environ un tiers des décès en Amérique du Nord. L'artère carotide, particulièrement la bifurcation carotide, est identifiée comme une source commune d'emboles qui se propagent vers le cerveau, bloquent l'écoulement sanguin local, et provoquent ainsi des accidents cérébrovasculaires. Ceci a mené à la mise en emphase de techniques diagnostiques servant à évaluer le risque d'accidents cérébrovasculaires dû à la maladie de l'artère carotide. Les techniques d'échographie Doppler (DUS, de l'anglais), en particulier, permettent la visualisation des patterns d'écoulement et la caractérisation de leurs divers paramètres. Pour améliorer nos connaissances de la façon avec laquelle les formes d'écoulement sanguin sont modifiées par la maladie de l'artère carotide les études de recherche sont habituellement effectuées avec l'aide de modèles vasculaires physiologiquement réalistes. Dans cet article, nous passons en revue le progrès qui a été accompli dans le développement de modèles vasculaires applicables aux ultrasons, et nous démontrons les possibilités des techniques DUS pour mesurer les patterns de vélocité, de turbulence, et de vorticité. Des systèmes d'écoulement applicables aux ultrasons ont été développés pour imiter la géométrie et l'hémodynamique de l'artère carotide dans des conditions normales et à diverses étapes du rétrécissement dû à l'athérosclérose. Ces systèmes in vitro fournissent un environnement contrôlé qui facilite le développement de nouvelles techniques diagnostiques, de même que l'étude et la caractérisation de l'écoulement sanguin en utilisant les techniques DUS. Des données obtenues pour des systèmes avec sténoses excentriques et concentriques et des systèmes avec sténoses altérés par l'introduction des dispositifs médicaux (endoprothèses vasculaires) ou de rugosité additionnelle (ulcération) sont présentées. Ces résultats démontrent la capacité des techniques cliniques d'échographie Doppler conventionnelles pour mesurer précisément la vitesse sanguine dans de petits volumes d'échantillons situés à l'intérieur de systèmes d'écoulement. Ceci permet de produire des cartes détaillées d'écoulement près et en aval de régions atteintes par la maladie vasculaire, ou de dispositifs d'intervention.

1. INTRODUCTION

Ultrasound (US) has become an invaluable diagnostic and therapeutic tool that is most appealing for its rapid accessibility and low cost compared to other modalities, such as x-ray computed tomography or magnetic resonance imaging. Ultrasound imaging uses high-frequency sound waves, typically 2-10 MHz, to form images of the internal body as a function of time and space. Similarly, Doppler ultrasound (DUS) techniques use high-frequency ultrasound in order to detect the presence of blood flow or to determine the velocity of the blood. The versatility of ultrasound for both anatomical imaging, flow visualization, and velocity measurement applications makes it a prime candidate for investigating vascular disease, particularly to elucidate the connections between local hemodynamics (blood flow) and vascular tissue changes, such as due to atherosclerosis.

Atherosclerosis, which is a thickening or hardening of the arteries forming plaques, promotes the development of blood clots or thrombosis by partial obstruction of the blood flow, elevated shear stresses, or plaque disruption. These clots, or displaced bits of plaque, form emboli that can travel downstream and block blood flow in smaller arteries of the brain, resulting in an ischemic stroke. Overall, stroke is the 4th leading cause of death in Canada, accounting for 7% of all deaths with an annual cost to the Canadian economy of about $2.7 billion (Heart and Stroke Foundation of Canada, 1999; Heart and Stroke Foundation of Canada, 2002). The carotid artery bifurcation in the human neck is a common site of atherosclerotic disease and is therefore highly relevant to stroke research. To determine the risk that a particular vessel poses, doctors will often examine a patient using x-ray imaging and measure the restriction of the vessel due to disease. However, the risk of producing a clot is not only due to the narrowing of the vessel lumen, but also the way that blood flows near the obstruction. It is believed that clot formation is accelerated in regions of slow or recirculating flow, high shear rate, and increased turbulence (Stein and Sabbah, 1974; Reininger et al., 1995; Holme et al., 1997). Doppler ultrasound has excellent potential as a tool to assess and visualize these flow features.

Doppler ultrasound can be used to study in vitro effects of various modeling parameters in order to gain a better understanding of the hemodynamics. This also helps to develop DUS further as a tool towards improved in vivo assessment of the hemodynamics. Ultimately it is desirable to determine if advanced flow parameters derived from DUS velocity measurements can be a better indicator of disease progression and more accurately reflect the absolute stroke risk due to plaque development, thrombus formation, or plaque rupture.

In this paper, we demonstrate the ability of DUS to visualize complex 2-D flow patterns and quantitatively assess mean velocity, turbulence intensity, and spectral broadening. Through the use of vascular models and simulated pulsatile blood-flow waveforms, it is then possible to use DUS to investigate flow features, such as turbulence and recirculation, that are relevant to stroke risk.

2. BACKGROUND

2.1: Carotid arterial disease diagnosis and treatment

Standard diagnosis of carotid arterial disease consists of assessment of the stenosis severity, or maximum vessel diameter reduction, where increasing stenosis severity indicates increased relative stroke risk. Standard treatment can vary from non-invasive drug therapy, such as anti-clotting agents, to invasive interventional procedures, such as carotid endarterectomy – a surgical procedure to remove the atherosclerotic plaque, or insertion of a stent – a mesh tube expanded to re-open the lumen and stabilize the carotid plaque.

While x-ray angiography is historically the gold standard for assessing stenosis severity, Doppler ultrasound has become increasingly popular as a non-invasive method to screen possible candidates for carotid endarterectomy. Several large multi-centre clinical trials have demonstrated the benefit of carotid endarterectomy, for symptomatic patients with severe stenosis (North American Symptomatic Carotid Endarterectomy Trial (NASCET), 1991; European Carotid Surgery Trialists' Collaborative, 1998), but also have acknowledged the role of other key factors, such as the presence of ulcerations (Eliasziw et al., 1994).

2.2: Role of B-mode Ultrasound Imaging in Assessing Vascular Disease

The use of B-mode ultrasound imaging has become increasingly popular for the diagnosis of carotid disease due to improved resolution and the development of 3-D ultrasound imaging techniques (Fenster et al., 1997). Ultrasound imaging, in general, can be used to see arterial geometry and patency, plaque severity and shape, plaque composition, and vessel stiffness, while 3-D B-mode ultrasound has been used to measure stenosis diameter, lumen morphology, and plaque volume in the carotid arteries (Griewing et al., 1996; Yao et al., 1998). Ultrasound has also proved to be more accurate than angiography in determining the presence or absence of ulceration (Van Damme and Vivario, 1993), where ulcerations are associated with increased stroke risk (Eliasziw et al., 1994; Rothwell et al., 2000).

2.3: Role of DUS for Flow Assessment

Doppler ultrasound is typically used to identify patients with high-velocity jets within the internal carotid artery, which is an indication of vessel narrowing or stenosis, and thus a surrogate measure of vessel lumen reduction. The maximum systolic velocity was first suggested as an indicator of carotid stenosis in 1979, with the rationale that due to regulation of cerebral blood flow, a reduction in lumen diameter will lead to an increase in blood velocity, at least until the increased flow resistance of the stenosis leads to a reduction in blood flow (Spencer and Reid, 1979). The peak systolic velocity (PSV) is the most commonly used DUS indicator, often combined with the end diastolic
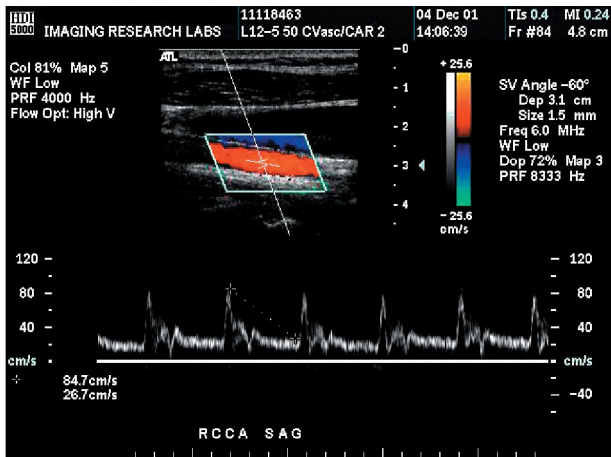
Figure 1: Example from a clinical ultrasound examination showing a B-mode (top centre) image with overlaid colour-encoded map of mean velocity (colour Doppler, shown in central box), along with a DUS spectrogram (bottom) of a sub-volume of velocities as a function of time over 5 cardiac cycles. The DUS sample volume is indicated by the crosshairs at the centre of the B-mode and colour-Doppler image.

velocity (EDV) to form a ratio (Moneta *et al.*, 1993; Schwartz *et al.*, 1997). These velocities may be assessed at the stenosis alone (Alexandrov *et al.*, 1997) or normalized by additional measurements in the common carotid artery (Arbeille *et al.*, 1999; Ranke *et al.*, 1999). Carpenter *et al.* (1996) give an excellent description of some commonly used velocity indices.

Pulsed Doppler ultrasound can be used to interrogate the blood velocities from a small finite sample volume (approx. 1-10 mm^3). A spectrogram (Fig. 1, bottom) is used to display the velocity as a function of time, where the range of velocities detected is shown along each vertical line with the energy content for each corresponding velocity encoded as the pixel intensity or brightness. Hence, a broad velocity range appears as a smeared vertical line.

The range of observed velocities is qualitatively used as an indication of the type of flow, since disturbed or turbulent flow will show a broader range of velocities for a given time point, but will also depend upon the size of the sample volume used. Pulsed DUS is limited to a relatively small sample volume (i.e. small spatial region of flow), and hence the user needs to move the sample volume around to sub-sample a larger volume.

One way to partially visualize the velocity spatial patterns over a larger volume is to use colour-Doppler techniques, which display estimates of the mean velocity as a colour-encoded map superimposed onto the B-mode image (see Fig. 1). However, current implementation is limited to reporting only the mean velocity, or similarly the integrated power for power-Doppler techniques; the mapping of peak velocity or other spectral information is not provided on standard clinical machines. Primarily, colour-Doppler ultrasound is used to assist with basic visualization of the 2-D flow field in order to ensure proper positioning of the smaller pulsed-Doppler sample volume (small cross-hair region within coloured map in Fig.1).

Arterial disease can lead to complicated flow including flow disturbances such as turbulence, vortices, and recirculation zones. Turbulence has also been shown to contribute to thrombus formation (Smith *et al.*, 1972; Stein and Sabbah, 1974). Regions of recirculation can lead to flow stagnation, with an increased risk of platelet aggregation and clot formation.

While velocity indices focus on the shape of the velocity waveform as a function of time over the cardiac cycle, they ignore the other information contained in the velocity-power spectrum that can be more difficult to assess, particularly in a quantitative manner, but are more indicative of factors such as flow disturbances. The use of additional information from Doppler ultrasound, other than peak systolic velocity in the stenosis, has been suggested to elucidate the local hemodynamics (Brown *et al.*, 1982; Rittgers *et al.*, 1983; Krause *et al.*, 1984; Kalman *et al.*, 1985; Cloutier *et al.*, 1996). Doppler ultrasound studies have demonstrated the potential for identifying various flow characteristics (such as flow separation, vortices, and turbulent regions) using various spectral parameters, such as spectral broadening (Brown *et al.*, 1982; Rittgers *et al.*, 1983), skewedness and kurtosis (Kalman *et al.*, 1985); turbulence intensity (Wu *et al.*, 1998); or turbulence-induced spectral (Bascom *et al.*, 1993) and power changes (Bascom *et al.*, 1997; Wu *et al.*, 1998).

2.4: *In vitro* studies

Experiments using flow visualization (LoGerfo *et al.*, 1981b; Ku and Giddens, 1983) and laser Doppler anemometry (LoGerfo *et al.*, 1981a; Ku and Giddens, 1987; Gijsen *et al.*, 1996) in carotid bifurcation models have clearly demonstrated some of the important flow characteristics such as flow separation, vortices, and turbulent regions. Interestingly, the carotid sinus bulb is the only part of the vascular system in which flow separation has been documented to occur (Nerem, 1992).

Most of the *in vitro* studies demonstrating turbulence or other unique flow characteristics have used simplified models of grids, 'Y'-shaped , 'T'-junction, or stenosed tubes. Stenotic vessels have typically been modeled as rigid-walled tubes with constrictions or orifices (Kim and Corcoran, 1974; Teague *et al.*, 1984). Carotid models have been either cast from averaged *in vivo* geometries representing a relatively disease-free vessel (Bharadvaj *et al.*, 1982) or cadaver specimens (Currie *et al.*, 1996) thus representing a specific case. Additionally, many flow studies use simplistic flow conditions such as steady flow or sinusoidally pulsatile flow. A comparison study by Lutz *et al.* (1983) demonstrated distinct differences in flow phenomena between steady, sinusoidal, and arterial pulsatile flow. Cavalcanti (1995) has discussed the limitations of such studies in modeling the *in vivo* flow system.

For *in vitro* flow studies to be most beneficial, it is important to replicate the range and complexity of flow regimes seen *in vivo* but in a controlled and systematic manner. Using a series of vascular models and ultrasound-
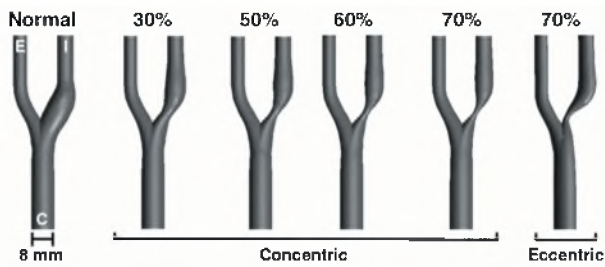
Figure 2: Idealized geometrical models of a carotid artery bifurcation (C=common carotid, I=internal carotid, E=external carotid) with a range of atherosclerotic plaque progression, leading from a normal (disease free) model to a severely stenosed model. Two configurations exist for each diseased model, representing symmetric (concentric) or asymmetric (eccentric) plaque development, as demonstrated by the two 70% stenosed models shown on the far right.

compatible phantoms, with an automated translational stage and acquisition system, it has been possible to study the flow patterns and changes corresponding to different model features. Thus it is possible to independently study the effects of various factors, such as: stenosis severity, stenosis shape, flow rate, flow resistance, the presence of ulcerations, ulceration size and geometry, or the introduction of vascular devices (e.g. stents).

3. METHODS

3.1: Models & phantoms

In vitro systems and phantoms offer a stable environment for developing and evaluating new techniques for investigating and characterizing flow. As part of an *in vitro* testing facility, a series of flow phantoms with representative geometries for various diseased states, compliance, and imaging properties has been developed. The geometrical models for the anthropomorphic carotid bifurcation phantoms are based on an *in vivo* characterization study of the carotid bifurcation by Smith *et al.* (1996) from x-ray arterial angiograms.

A family of models was derived to represent average carotid bifurcation geometries with progressing stenosis severity from a disease free (i.e. normal) geometry to mild (30%), moderate (50, 60%), and severe stenosis (70% and greater). Stenosis severity, at the point of maximum stenosis, is classified according to the NASCET criteria of percent diameter difference relative to the downstream ICA. Two sets of models exist with a different stenosis eccentricity representing different extremes in terms of plaque symmetry: a concentric model simulates a symmetrical plaque buildup within the lumen of a normal (i.e. disease free) geometry, whereas an eccentric model simulates a preferential buildup progressing inward from the lateral internal carotid artery wall. Selected geometrical models are shown in Fig. 2. As plaque builds up within a normal arterial wall, it impinges upon the arterial lumen, leaving less residual lumen for the blood flow. The geometries shown in Fig. 2 represent the residual flow lumen, such that the spatial difference between the normal

model and a given stenosed model comprises the actual plaque volume.

The models can be incorporated into different types of materials. For the results shown here, we used a combination of two different methods for creating three different types of phantoms for different types of studies or for different imaging modalities. The methods include using a numerically controlled milling system and a lost-core casting technique (Smith *et al.*, 1999; Poepping *et al.*, 2004). To use these techniques to reproduce the desired geometries requires arbitrarily mouldable materials or a smoothly millable block of material. Typically this demands some compromise in properties in order to have sufficient strength to survive physiological flow pressures, reasonable modality-specific properties (e.g. tissue-mimicking acoustic properties), and ease of fabrication.

The different types of phantoms produced include: 1) a distensible, thin-walled silicone artery embedded in a gel-based tissue-mimicking material (Smith *et al.*, 1999; Poepping *et al.*, 2004), 2) an optically transparent silicone block phantom for particle-imaging techniques (Shelley Medical Imaging Technologies, London, ON), and 3) rigid ultrasound-compatible polymer phantoms.

The compliant gel-based phantoms provide a controlled, yet physiologically realistic, system for investigating how flow patterns change in a series of models that emulate typical disease progression. Here, good ultrasound compatibility is important in order to study corresponding changes in observed Doppler ultrasound spectra, and thus testing the abilities of Doppler ultrasound to identify important flow characteristics. The thin-walled silicone artery provides sufficient strength to withstand physiologically realistic pressures, and it is surrounded by an ultrasound-compatible, tissue-mimicking material (Ramnarine *et al.*, 2001).

The optically transparent silicone phantoms are comprised of a single block of silicone elastomer with a hollow flow channel with the desired carotid geometry. These phantoms are used for particle imaging techniques enable direct visualization of the complex flow patterns. Experiments using the gel-based and silicone phantoms in turn have provided for excellent comparison studies with computational fluid dynamics (CFD) (Steinman *et al.*, 2000; Khoshniat *et al.*, 2005) using identical geometrical models.

The carotid models, or other geometries, can also be milled directly into an ultrasound-compatible polymer. This technique was used in order to incorporate models of ulcerations in the geometries, test patient-specific geometries, and to test intravascular devices. With this technique, additional surface roughness and fine features, which are difficult to reproduce with a lost-core casting technique, can be precisely fabricated. Also the technique is far less time consuming than the numerous steps involved in the lost-core casting techniques required for gel-based or silicone phantoms. These plastic phantoms are useful when the goal is a direct comparison between a control model and a test model, i.e. to investigate relative flow differences due to an additional geometrical feature (e.g. ulceration) or
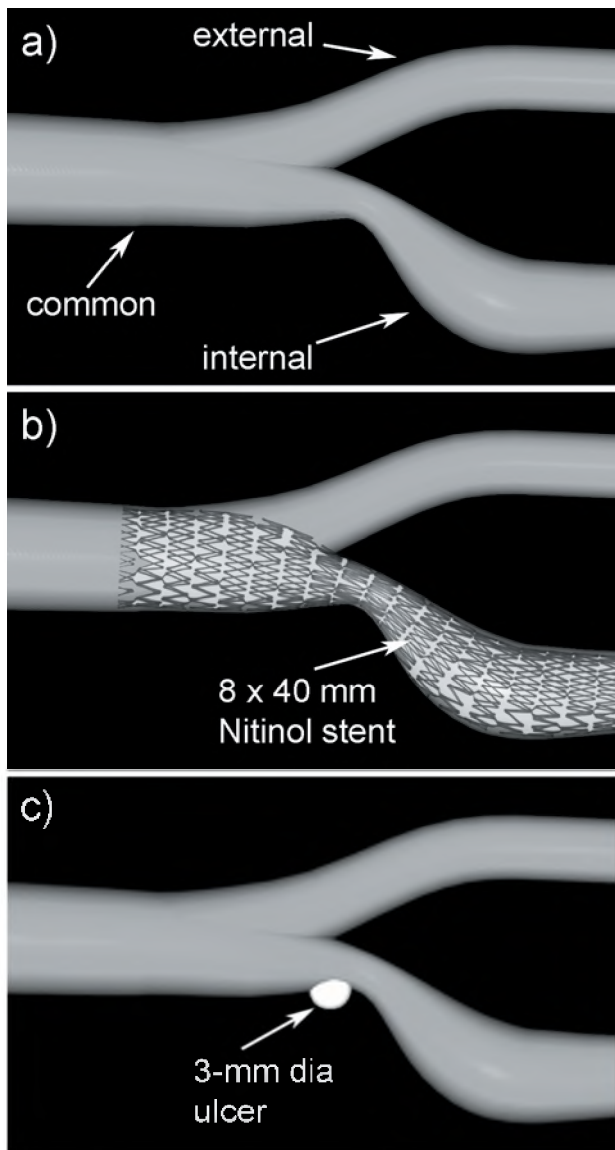
Figure 3: Schematic demonstrating a 50% eccentric carotid model before (a) and after (b) stent implantation, and (c) an identical model with a 3-mm diameter hemispherical ulceration in ICA branch extending into the impinging plaque volume.

intravascular device (e.g. stent). Hence, possible problems with refraction errors due to the differences in the material's acoustic properties are not a significant issue because of the comparative nature of the study. Additionally, the design of the rigid phantoms makes it possible to deploy a stent, for example, and later extract it for re-use, without sacrificing the integrity of the phantom.

In the study described here, a plastic phantom with 50% eccentric carotid model geometry was used to investigate the possible flow disturbances due to a stent implantation. A self-expanding Nitinol carotid stent (Cordis PRECISE, 8x40mm) was used, which extended from the common carotid artery (CCA) into the internal carotid artery (ICA), covering the external carotid artery (ECA) orifice or branch, as shown in Fig. 3b. DUS

measurements were performed before and after stent implantation.

Additionally, an identical 50%-eccentric model phantom was produced with a 3-mm diameter hemispherical ulcer located on the non-flow-divider wall of the ICA at the level of the bifurcation apex, as shown in Fig. 3c.

Finally, for testing the detection of different levels of turbulence, an orifice phantom was used consisting of a 1.2-m long acrylic inlet tube with a 1.27-cm inner diameter, which was connected to a mountable interface that accepted different inserts. A 1.53-mm thick disk with a 1.6-mm diameter orifice in the center was inserted to generate constrained-jet turbulence. The long inlet length ensured fully developed laminar flow prior to the orifice. An ultrasound-compatible high-density polyethylene portion, with a 1.27-cm inner diameter and 1.9-cm outer diameter, was connected to the interface, which enabled DUS measurements up to 8 cm downstream of the orifice.

3.2: *In vitro* facility

A programmable system was used for semi-automated data acquisition over 3-D space and multiple cardiac cycles with temporal (i.e. ECG-like) gating (Poepping *et al.*, 2002). A 3-axis translational stage allowed the lumen to be interrogated with a small Doppler sample volume at the desired spatial intervals in a 3-D raster to collect 10 cardiac cycles of gated Doppler signal at each site. Thus, it is possible to collect high-resolution DUS data over a full carotid artery volume for an extended length of time. To interrogate a carotid bifurcation model at 1-mm increments, the central plane consisted of over 1000 sites, and a half-volume data set consisted of over 3200 sites.

For the steady flow experiments with the 1.6-mm orifice, 1 s of data was collected at each point within a 2-D central vertical plane, starting 1.7 cm distal to the orifice and extending 4 cm downstream producing a complete 2-D grid of 533 points with 1-mm sample spacing.

A programmable computer-controlled pump (Holdsworth *et al.*, 1991) (UHDC Flow System, Shelley Medical Imaging Technologies, London, ON) was used to perfuse the phantoms with an appropriate fluid, as described in each of the DPI and DUS sections below. The pump can be programmed to output constant or pulsatile flow including arbitrary flow waveforms, for example, to simulate the *in vivo* carotid artery waveform (Holdsworth *et al.*, 1999). For the steady flow experiments, flow rates of 5, 7.5, 10, 12.5, and 15 ml/s were used. For the pulsatile flow studies, a carotid waveform was used with a mean flow rate of 6 ml/s and peak flow rate at peak systole of 23.5 ml/s.

3.3: Doppler ultrasound (DUS)

For DUS studies, the phantoms were perfused with an ultrasound-compatible blood-mimicking fluid (Ramnarine *et al.*, 1998) with specified attenuation of 0.26 dB/cm at 5 MHz, speed of sound of 1547 m/s, and viscosity of 4.1 ± 0.1
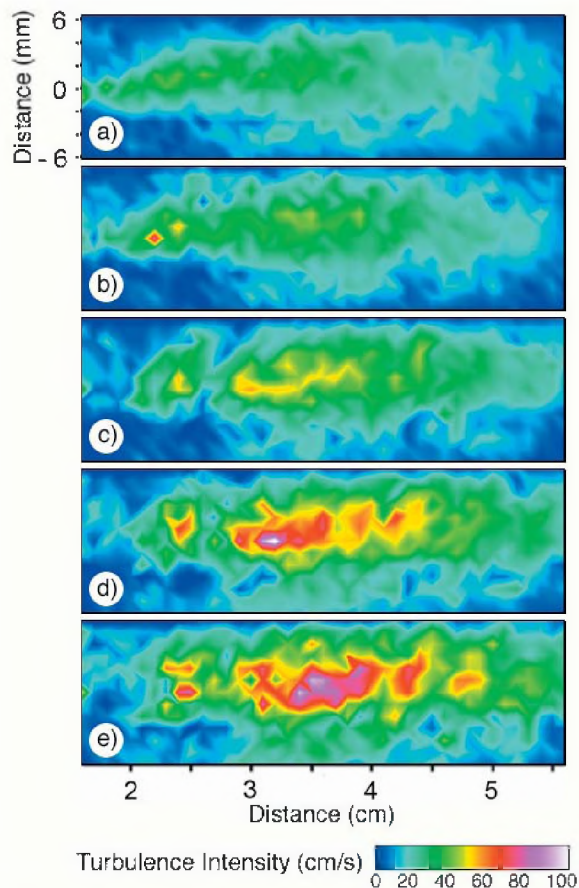
Figure 4: Colour-encoded, 2-D map of turbulence intensity for flow rates 5, 7.5, 10, 12.5, and 15 ml/s (a to e respectively) acquired 1.7 to 5.7 cm downstream of a 1.6-μm orifice.

mPa·s. The BMF has 5±2 μm nylon particles (Orgasol 2001 UD NAT 1, Elf Atochem, Paris, France) that act as Doppler scattering sites.

Data was collected using one of two conventional clinical ultrasound systems: 1) ATL Ultramark 8 (Bothell, WA), 5 MHz mechanical scanning probe (Access 10-PV), 1.5-mm sample-volume length, collecting quadrature data, 23 kHz pulse repetition frequency (PRF); or 2) ATL Ultramark 9, L7-4 (4 MHz central frequency) linear array transducer, 1.0-mm sample-volume length, collecting audio data, 18.5 kHz PRF. Acquisition parameters used were a Doppler angle of 60°, minimum sample volume length, and a minimum 50 Hz wall filter. Data was digitized at 44.1 kHz and recorded for offline analysis, including a 1024-point FFT with a 1024-point Hanning window and a 50% overlap between consecutive windows.

Spectra were analyzed with respect to mean velocity, peak velocity (velocity corresponding to 90% power), integrated power, or spectral broadening index, SBI (given by: 1 − mean velocity/peak velocity) (Brown et al., 1982). Thus, a 4-D (i.e. time-varying 3-D) Doppler data set with 1.3-cm/s velocity (43 Hz frequency) resolution and 12-ms temporal resolution (approximately 79 time points per cardiac cycle) can be produced for each parameter. The data was prospectively gated, such that it was possible to

derive an ensemble-averaged waveform (1 average cycle from the 10 measured cycles), for each of the spectral parameters, as well as the root-mean-square (RMS) deviation in the 10 contributing values at each time point in the ensemble-averaged waveform. Using this technique, turbulence intensity (TI) was calculated, corresponding to the RMS deviation in the mean velocity for each time point.

3.4: Digital Particle Imaging (DPI)

Digital particle imaging (DPI) is a well-established technique that is valuable as a means of visualizing the 3-D flow patterns and as a reference for comparison with the DUS data. Flow can be visualized in transparent phantoms of identical model geometry as used in DUS and CFD studies (Steinman et al., 2000; Poepping et al., 2001). The DPI system consisted of two 5 mW He-Ne lasers (Melles Griot, Carlsbad, CA) to produce 1-mm-thick fanbeams that illuminated the central plane of the carotid model uniformly from opposite sides. A charge-coupled-device (CCD) camera (Panasonic GP-MF552, Seacaucus, NJ) was used to record the flow of small (~400 μm diameter) reflective polystyrene particles (Amberlite IRA-904, Sigma-Aldrich, Oakville, ON) in a 2:1 mixture by volume of water-glycerol fluid. ECG-gated, 640x480, de-interlaced digital images of the central plane of the vessel model were obtained with 17 ms temporal resolution using a UNIX workstation (SGI Indy, Silicon Graphics Inc., Mountainview, CA).

4. RESULTS:

Figure 4 shows the turbulence intensity measured downstream of a 1.6-mm orifice, demonstrating the ability to quantify turbulence. The fluctuation due to standard noise, measured from a site within fully developed laminar flow (i.e. without orifice insert) was found to be 0.7 cm/s. Fig. 4 shows that for the 5 and 7.5 ml/s steady-flow rates, TI values in the jet were in the range of 30-50 cm/s, but extended up to approximately 100 cm/s at the higher flow rates of 12.5 and 15 ml/s.

It is relevant to note that the pulsatile carotid waveform used in the vascular models has a mean flow rate of 6 ml/s and maximum of 23.5 ml/s at peak systole. It is also relevant to note that for the 70% stenosed model, the diameter at the point of maximum stenosis corresponds to 1.68 mm, although with a significantly longer stenotic neck than the 1.53-mm thickness of the orifice plate used above.

Figure 5 shows results for two severely (70%) stenosed models in a comparison of DPI flow maps and 2-D central-plane maps for three different DUS spectral parameters – mean velocity, spectral broadening index, and turbulence intensity. The models differ only in the shape of the stenosis, representing a different symmetry in the buildup of plaque. The DPI data provides an important reference for identifying the flow features. Since the DPI image represents a 17-ms snapshot, each black streak traces out the path of a particle within the illuminated central plane, and the length of the particle streak is representative of the velocity. Slow or stagnant particles appear as spots. From

Fig. 5a and 5b, it can be seen that the severely stenosed models exhibit a jet stream with resultant recirculation zones on both sides of the jet and highly disturbed, or turbulent, flow downstream. However, the recirculation zones differ considerably in size. The eccentric model exhibits a larger recirculation zone ER1 and with a higher gradient of velocities (i.e. higher SBI in Fig. 5f). Recall that the SBI is determined from the velocity distribution within each approximately 1-mm^3 sample volume. The four vertical panels present different but highly complementary results. The mean velocity maps are a quantitative indication of the jet velocity, as well as the general flow behaviour. The SBI maps clearly indicate the regions of recirculation (i.e. spatial variance) and the TI maps indicate rapidly fluctuating or unstable flow (i.e. temporal variance). Note that the TI here for peak systole (i.e. peak flow of 23.5ml/s) is on the order of 50 cm/s with values extending up to 120 cm/s. Similar flow pattern comparisons have been possible using DPI and CFD (Steinman *et al.*, 2000), CFD and DUS (Khoshniat *et al.*, 2005), and DPI and DUS (Poepping *et al.*, 2001).

Figure 6 shows the mean velocity maps and Fig. 7 the turbulence intensity maps comparing results from the three 50%-eccentric models studied here: i) before (Fig 6a, 7a) and ii) after (Fig 6b, 7b) stent implantation and iii) with a 3-mm diameter hemi-spherical plaque ulceration (Fig. 6c, 7c). The results indicate that the introduction of a self-expanding carotid stent did not have a significant effect on the measurements of mean velocity and turbulence intensity when geometry, flow rate, and Doppler parameters were maintained. Figures 6a and 6b exhibit very similar velocity patterns through the stenosis and the ICA. Slightly lower velocities can be observed in the neck of the stenosis and, in particular, in the ECA (upper branch), after flow has passed through the mesh wall of the stent, but it appears to quickly re-laminarize, as indicated by a parabolic-like colour gradient. More notably, the TI maps in Fig. 7a and 7b do not suggest notably higher levels of flow disturbance downstream in the ICA.

Finally, Fig. 6c and 7c represent mean velocity and TI flow maps for the 50%-eccentric model with an ulceration, which can also be compared with Fig. 6a and 7a of the standard (ulcer-free) 50%-eccentric model. Fig. 6c and 7c indicate that the imposed ulceration did not introduce obvious changes in downstream velocity patterns or flow disturbance.
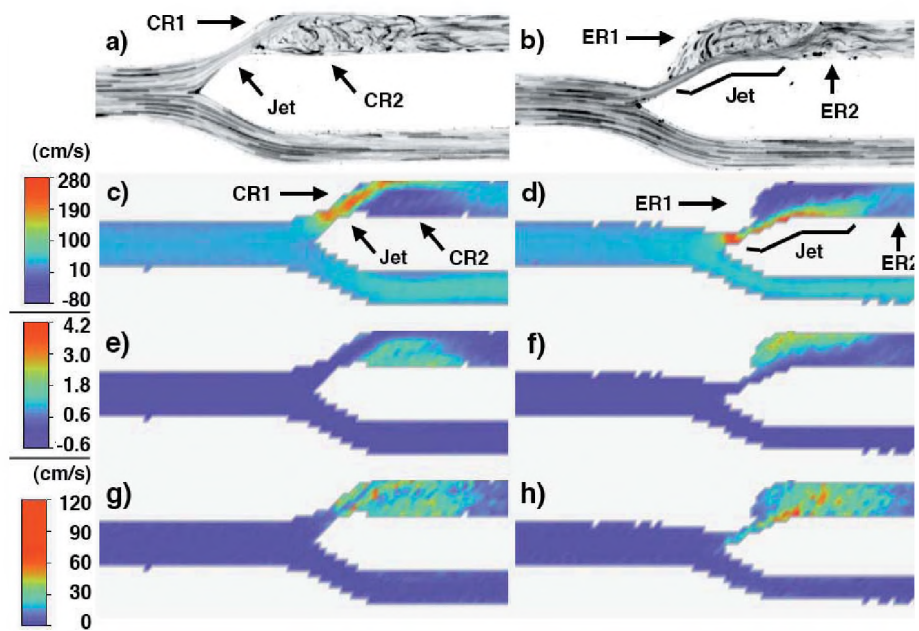
Figure 5: Comparison of DPI and DUS flow maps for carotid bifurcation models with 70% concentric stenosis (left panels) and 70% eccentric stenosis (right panels) at peak systole. Panels show DPI (a,b), DUS mean velocity (c,d), DUS spectral broadening index (e,f), and DUS turbulence intensity (g,h) with corresponding colour bar on the far left. Flow proceeds from the common carotid artery (left) and divides into the internal (top) and external (bottom) carotid arteries. The different jet paths and recirculation zones are indicated in the concentric (CR1, CR2) and eccentric (ER1, ER2) models, respectively.
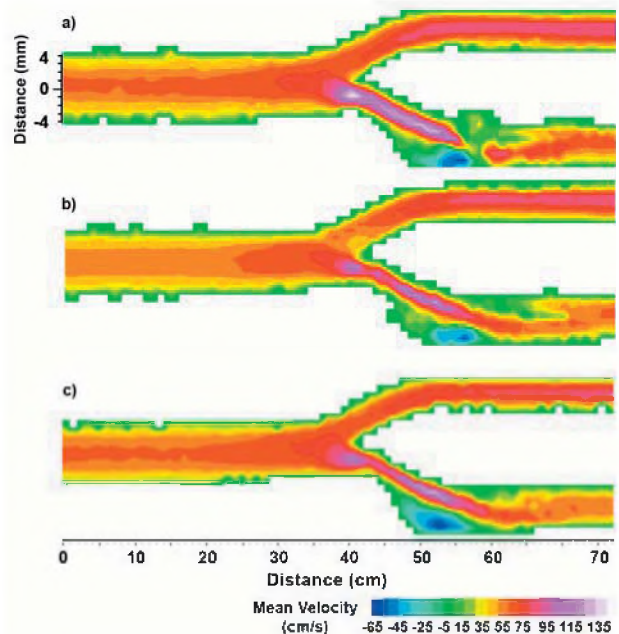
Figure 6: Colour-encoded mean velocity maps of flow in a carotid bifurcation with 50% concentric stenosis model: a) control model (no modification), b) with intravascular stent, and c) with a 3-mm diameter ulceration, as shown in Fig. 3. Flow from the common carotid artery on the left branches into the external (top) and internal (bottom) carotid arteries.
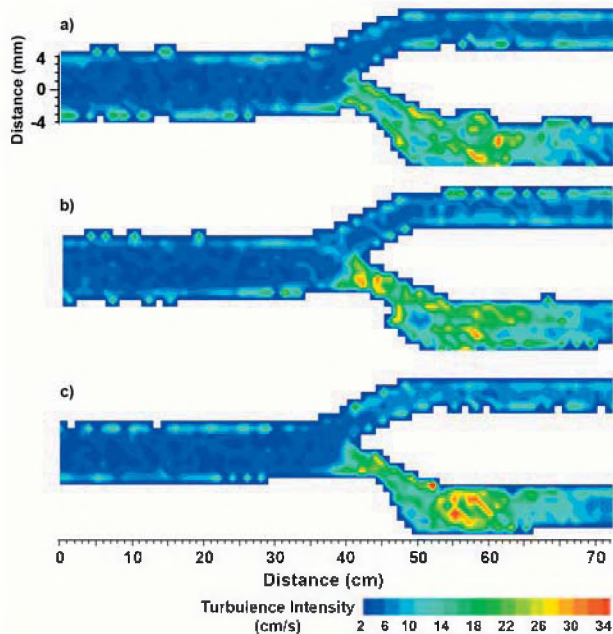
Figure 7: Colour-encoded turbulence intensity maps of flow in a carotid bifurcation with 50% concentric stenosis model: a) control model (no modification), b) with intravascular stent, and c) with a 3-mm diameter ulceration, as shown in Fig. 3. Flow from the common carotid artery on the left branches into the external (top) and internal (bottom) carotid arteries.

5. DISCUSSION & CONCLUSION

A major limitation of the current clinical implementation of DUS diagnoses of carotid disease based on peak velocities in the stenosis is that this only provides a partial description of the hemodynamic disturbances caused by the stenosis. High blood-flow velocities are only indirectly related to stroke and thrombo-embolus production. Elevated shear stress rates, the formation of turbulence, and the presence of slow or recirculating flow have all been implicated in increased clot production. Therefore other hemodynamic parameters, such as shear and turbulence, may be more directly correlated with thromboembolism production and plaque rupture in the carotid artery. Doppler ultrasound may in fact provide a more direct measurement of stroke risk based on hemodynamic factors compared to current techniques based strictly on lumen diameter reduction or some other surrogate measure.

The use of pulsatile flow is particularly important for studies in vascular models. Although the data here only shows a particular snapshot in time, the complete data set can be viewed as a cine loop or movie. By viewing the whole time sequence, the recirculation zones can be seen to form and then get flushed out, and similarly the turbulence dissipates and reforms through the cardiac cycle. Additionally, it is possible to see vortex shedding occur, particularly from the downstream recirculation zone (CR2 in Fig. 5) of the concentric model.

It is important to note that all of the ultrasound data we report was acquired with conventional clinical ultrasound equipment. This approach provides a major advantage, bringing the research one step closer to translating the work to *in vivo* studies. The DUS work shown here all has a direct application to human studies in future work, such as evaluating *in vivo* flow following carotid endarterectomy, following insertion of intravascular devices, or for improved diagnosis of vascular disease.

Future *in vitro* work can include the testing of patient-specific models using the rapid prototyping method of milling geometries directly into plastics or other materials. Also, while the ulceration model that was shown here did not introduce significant changes in downstream velocity patterns, this particular model only represents one typical category of ulceration geometry. Future work will investigate ulcerations of other geometries, including cavities with different alignment relative to the flow direction (i.e. upstream or downstream), or geometries with an obvious neck extending between the ulcer cavity and the residual lumen. Additionally, it may be desirable to further test intravascular devices in more compliant models where the stent may affect the compliance, which leads to a change in flow resistance and the velocity waveform.

The overall goal has been the development of a test facility to provide a means of evaluating and investigating various hemodynamic effects correlated with vascular disease.

ACKNOWLEDGEMENTS

REFERENCES

Alexandrov AV, Vital D, Brodie DS, Hamilton P and Grotta JC. 1997 Grading carotid stenosis with ultrasound. An interlaboratory comparison. *Stroke* 28:1208-10

Arbeille P, Bouin-Pineau MH and Herault S. 1999 Accuracy of the main Doppler methods for evaluating the degree of carotid stenoses (continuous wave, pulsed wave, and color Doppler). *Ultrasound in Medicine & Biology* 25:65-73

Bascom PA, Cobbold RS, Routh HF and Johnston KW. 1993 On the Doppler signal from a steady flow asymmetrical stenosis model: effects of turbulence. *Ultrasound in Medicine & Biology* 19:197-210

Bascom PA, Johnston KW, Cobbold RS and Ojha M. 1997 Relation of the flow field distal to a moderate stenosis to the Doppler power. *Ultrasound in Medicine & Biology* 23:25-39

Bharadvaj BK, Mabon RF and Giddens DP. 1982 Steady flow in a model of the human carotid bifurcation. Part I--flow visualization. *Journal of Biomechanics* 15:349-62

Brown PM, Johnston KW, Kassam M and Cobbold RS. 1982 A critical study of ultrasound Doppler spectral analysis for

detecting carotid disease. *Ultrasound in Medicine & Biology* 8:515-23

Carpenter JP, Lexa FJ and Davis JT. 1996 Determination of duplex Doppler ultrasound criteria appropriate to the North American Symptomatic Carotid Endarterectomy Trial. *Stroke* 27:695-9

Cavalcanti S. 1995 Hemodynamics of an artery with mild stenosis. *Journal of Biomechanics* 28:387-99

Cloutier G, Allard L and Durand LG. 1996 Characterization of blood flow turbulence with pulsed-wave and power Doppler ultrasound imaging. *Journal of Biomechanical Engineering* 118:318-25

Currie IC, Wilson YG, Baird RN and Lamont PM. 1996 Detection of sub-critical arterial stenoses by hyperaemic Doppler. *European Journal of Vascular & Endovascular Surgery* 11:29-35

Eliasziw M, Streifler JY, Fox AJ, *et al.* 1994 Significance of plaque ulceration in symptomatic patients with high-grade carotid stenosis. North American Symptomatic Carotid Endarterectomy Trial. *Stroke* 25:304-8

European Carotid Surgery Trialists' Collaborative G. 1998 Randomised trial of endarterectomy for recently symptomatic carotid stenosis: final results of the MRC European Carotid Surgery Trial (ECST). *Lancet* 351:1379-87

Fenster A, Lee D, Sherebrin S, *et al.* 1997 *Three-dimensional ultrasound imaging of carotid occlusive disease,* (Amsterdam: Elsevier) pp 17-24

Gijsen FJ, Palmen DE, van der Beek MH, *et al.* 1996 Analysis of the axial flow field in stenosed carotid artery bifurcation models--LDA experiments. *Journal of Biomechanics* 29:1483-9

Griewing B, Morgenstern C, Driesner F, *et al.* 1996 Cerebrovascular disease assessed by color-flow and power Doppler ultrasonography. Comparison with digital subtraction angiography in internal carotid artery stenosis. *Stroke* 27:95-100

Heart and Stroke Foundation of Canada H 1999 The changing face of heart disease and stroke in Canada. (Ottawa, Canada

Heart and Stroke Foundation of Canada H 2002 (HSFC Homepage).

Holdsworth DW, Norley CJ, Frayne R, Steinman DA and Rutt BK. 1999 Characterization of common carotid artery blood-flow waveforms in normal human subjects. *Physiological Measurement* 20:219-40

Holdsworth DW, Rickey DW, Drangova M, Miller DJ and Fenster A. 1991 Computer-controlled positive displacement pump for physiological flow simulation. *Medical & Biological Engineering & Computing* 29:565-70

Holme PA, Orvim U, Hamers MJ, *et al.* 1997 Shear-induced platelet activation and platelet microparticle formation at blood flow conditions as in arteries with a severe stenosis. *Arteriosclerosis, Thrombosis & Vascular Biology* 17:646-53

Kalman PG, Johnston KW, Zuech P, Kassam M and Poots K. 1985 In vitro comparison of alternative methods for quantifying the severity of Doppler spectral broadening for the diagnosis of carotid arterial occlusive disease. *Ultrasound in Medicine & Biology* 11:435-40

Khoshniat M, Thorne ML, Poepping TL, *et al.* 2005 Real-time numerical simulation of Doppler ultrasound in the presence of nonaxial flow. *Ultrasound in Medicine and Biology* 31:519-28

Kim BM and Corcoran WH. 1974 Experimental measurements of turbulence spectra distal to stenoses. *Journal of Biomechanics* 7:335-42

Krause H, Segard M, Carey P, Bernstein EF and Fronek A. 1984 Doppler power frequency spectrum analysis in the diagnosis of carotid artery disease. *Stroke* 15:351-8

Ku DN and Giddens DP. 1983 Pulsatile flow in a model carotid bifurcation. *Arteriosclerosis* 3:31-9

Ku DN and Giddens DP. 1987 Laser Doppler anemometer measurements of pulsatile flow in a model carotid bifurcation. *Journal of Biomechanics* 20:407-21

LoGerfo FW, Crawshaw HM, Nowak M, *et al.* 1981a Effect of flow split on separation and stagnation in a model vascular bifurcation. *Stroke* 12:660-5

LoGerfo FW, Nowak MD, Quist WC, Crawshaw HM and Bharadvaj BK. 1981b Flow studies in a model carotid bifurcation. *Arteriosclerosis* 1:235-41

Lutz RJ, Hsu L, Menawat A, Zrubek J and Edwards K. 1983 Comparison of steady and pulsatile flow in a double branching arterial model. *Journal of Biomechanics* 16:753-66

Moneta GL, Edwards JM, Chitwood RW, *et al.* 1993 Correlation of North American Symptomatic Carotid Endarterectomy Trial (NASCET) angiographic definition of 70% to 99% internal carotid artery stenosis with duplex scanning. *Journal of Vascular Surgery* 17:152-7; discussion 7-9

Nerem RM. 1992 Vascular fluid mechanics, the arterial wall, and atherosclerosis. *Journal of Biomechanical Engineering* 114:274-82

North American Symptomatic Carotid Endarterectomy Trial C. 1991 Beneficial effect of carotid endarterectomy in symptomatic patients with high-grade carotid stenosis. *New England Journal of Medicine* 325:445-53

Poepping TL, Nikolov HN, Rankin RN, Lee M and Holdsworth DW. 2002 An in vitro system for Doppler ultrasound flow studies in the stenosed carotid artery bifurcation. *Ultrasound in Medicine and Biology* 28:495-506

Poepping TL, Nikolov HN, Thorne ML and Holdsworth DW. 2004 A thin-walled carotid vessel phantom for Doppler ultrasound flow studies. *Ultrasound in Medicine & Biology* 30:1067-78

Poepping TL, Rankin RN and Holdsworth DW. 2001 Four-dimensional Doppler ultrasound measurements in stenosed carotid bifurcation models: Effect of concentric vs. eccentric stenosis. Proc. of SPIE Medical Imaging 2001: Ultrasonic Imaging and Signal Processing, ed. MF Insana and KK Shung. 4325:305-13

Ramnarine KV, Anderson T and Hoskins PR. 2001 Construction and geometric stability of physiological flow rate wall-less stenosis phantoms. *Ultrasound in Medicine & Biology* 27:245-50

Ramnarine KV, Nassiri DK, Hoskins PR and Lubbers J. 1998 Validation of a new blood-mimicking fluid for use in Doppler flow test objects. *Ultrasound in Medicine & Biology* 24:451-9

Ranke C, Creutzig A, Becker H and Trappe HJ. 1999 Standardization of carotid ultrasound: a hemodynamic method to normalize for interindividual and interequipment variability. *Stroke* 30:402-6

Reininger AJ, Reininger CB, Heinzmann U and Wurzinger LJ. 1995 Residence time in niches of stagnant flow determines fibrin clot formation in an arterial branching model--detailed flow analysis and experimental results. *Thrombosis & Haemostasis* 74:916-22

Rittgers SE, Thornhill BM and Barnes RW. 1983 Quantitative analysis of carotid artery Doppler spectral waveforms: diagnostic value of parameters. *Ultrasound in Medicine & Biology* 9:255-64

Rothwell PM, Gibson R and Warlow CP. 2000 Interrelation between plaque surface morphology and degree of stenosis on carotid angiograms and the risk of ischemic stroke in patients with symptomatic carotid stenosis. On behalf of the European Carotid Surgery Trialists' Collaborative Group. *Stroke* 31:615-21

Schwartz SW, Chambless LE, Baker WH, *et al.* 1997 Consistency of Doppler parameters in predicting arteriographically confirmed carotid stenosis. *Stroke* 28:343-7

Smith RF, Rutt BK, Fox AJ, Rankin RN and Holdsworth DW. 1996 Geometric characterization of stenosed human carotid arteries. *Academic Radiology* 3:898-911

Smith RF, Rutt BK and Holdsworth DW. 1999 Anthropomorphic carotid bifurcation phantom for MRI applications. *Journal of Magnetic Resonance Imaging* 10:533-44

Smith RL, Blick EF, Coalson J and Stein PD. 1972 Thrombus production by turbulence. *Journal of Applied Physiology* 32:261-4

Spencer MP and Reid JM. 1979 Quantitation of carotid stenosis with continuous-wave (C-W) Doppler ultrasound. *Stroke* 10:326-30

Stein PD and Sabbah HN. 1974 Measured turbulence and its effect on thrombus formation. *Circulation Research* 35:608-14

Steinman DA, Poepping TL, Tambasco M, Rankin RN and Holdsworth DW. 2000 Flow Patterns at the Stenosed Carotid Bifurcation: Effect of Concentric Versus Eccentric Stenosis. *Annals of Biomedical Engineering* 28:415-23

Teague SM, von Ramm OT and Kisslo JA. 1984 Pulsed Doppler spectral analysis of bounded fluid jets. *Ultrasound in Medicine & Biology* 10:435-41

Van Damme H and Vivario M. 1993 Pathologic aspects of carotid plaques: surgical and clinical significance. *International Angiology* 12:299-311

Wu SJ, Shung KK and Brasseur JG. 1998 In situ measurements of Doppler power vs. flow turbulence intensity in red cell suspensions. *Ultrasound in Medicine & Biology* 24:1009-21

Yao J, van Sambeek MR, Dall'Agata A, *et al.* 1998 Three-dimensional ultrasound study of carotid arteries before and after endarterectomy; analysis of stenotic lesions and surgical impact on the vessel. *Stroke* 29:2026-31.